CrossMark

Thermogravimetric study of the reduction of copper slag by biomass

Reduction characteristics and kinetics

Zongliang Zuo[1] · Qingbo Yu[1] · Mengqi Wei[1] · Huaqing Xie[1] · Wenjun Duan[1] ·
Kun Wang[1] · Qin Qin[1]

Abstract The utilization of copper slag is an attractive option of iron resource. However, extra energy consumption is required and contributes to greenhouse gases. In this paper, biomass was introduced as a new kind of reductant for the reduction of copper slag to decrease the energy consumption. The reduction kinetics and reduction characteristics of three kinds of biomasses were studied by thermogravimetric analyzer (TG). The TG curves showed the reduction reaction of copper slag and biomass could be divided into three stages during heating process: drying and pyrolysis of biomass process (<959 K), pre-reduction process (959–1100 K) and reduction reaction process (>1100 K). Pine sawdust showed the best reducing property and the reduction ratios of pine sawdust, corncob and straw reached to 80.6, 76.1, and 60.0 %, respectively, when the mass ratio of biomass/slag was 2:1. As the additive, CaO had promotion effects on the reduction reaction. With the increase in CaO addition, the reduction ratio of copper slag increased firstly and reached a peak at CaO/slag was 0.3:1 and then it declined due to the changes of slag viscosity. By kinetics analysis, the reduction reaction confirmed well with shrinking core model (R1). The activation energy of reactions was affected by the addition of biomass and heating rate in experiments. With the increase in the addition of biomass, the activation energy of reduction reaction increased gradually; with the increase in heating rate, the activation energy of reduction reaction decreased.

✉ Qingbo Yu
yuqb@smm.neu.edu.cn

[1] School of Materials and Metallurgy, Northeastern University, P.O. Box 345, No 11, Lane 3, Wenhua Road, Heping District, Shenyang 110819, Liaoning, People's Republic of China

Introduction

As an important part of metallurgy industry, copper smelting is an industry of intensive energy and resource. In recent years, the production of copper has been grown rapidly and the production of copper reached 20.4 million tons annual [1]. It has been estimated that about 2–3 tons of slag is generated for every ton of copper produced [2]. Copper smelting slag contains large amount of heat and some valuable metals (Fe, Cu, Zn, et al. as listed in Table 1), in which the content of iron could reach to 45 % [2]. It means that up to 26.8 million tons of potential Fe was produced in copper slag every year.

At present, copper slag is treated by water-quenched traditionally and widely used in the sand-blasting industry or used as some value-added products, such as cement, concrete, fill, abrasive tools, abrasive materials, mineral wool and glass ceramics [3, 4]. However, the waste heat and valuable metals cannot be recovered by this method. Besides, water-quenched method wastes large amount of water and can produce toxic wastes which can pass into atmosphere.

Based on the shortage of high-grade iron ore resources in recent years, different recovery methods have been studied to recover iron from copper slag. These methods include reduction method [5–9], oxidation method [10, 11], grinding flotation method [12], and magnetic separation method [13]. Due to the limits of economic, application of these methods does not result in significant results of the disposed slag. Oxidation and reduction methods had the potentiality to realize the waste heat recovery of copper

Table 1 The compositions of copper slag, mass%

FeO	Fe$_3$O$_4$	CaO	Al$_2$O$_3$	MFe	SiO$_2$	Cu	MgO	S	Zn	Others
37.50	18.90	0.23	0.98	1.24	31.99	0.74	0.42	0.39	2.78	4.87

slag. Usually, oxidation method is used in combination with other separation methods, and air or oxygen is injected into slag pond in this method. Under oxidizing conditions, the main phase of copper slag would convert from fayalite to magnetite, which will be separated by magnetic separation method, flotation method, or leaching method. By contrast, reduction method recovers iron by adding different kinds of reductants and it has the advantage of high Fe recovery and low pollution to the environment. The characteristics of different reductant have different effects on the reduction results.

With respect to the reduction characteristics of different kinds of reductants, studies had been carried out. The types of reductants fell into two major categories, solid reductants and gas reductants. As research objects of solid reductants, coal, coke, graphite, coal ash and anthracite dust had been applied to recover iron from copper smelting slag. Extensive researches have been conducted in reaction mechanism and kinetics [7–9, 14–16]. The reduction mechanism and kinetics of copper slag included the chemical reaction steps, reduction rate, and mass transfer in slag, solid carbon and gas bubble. The rate-limiting step of reduction reaction was affected by the contents of FeO and carbon types. Moreover, gas reductants include H$_2$, CO, CH$_4$, and gas mixture (such as natural gas) [6, 17, 18]. Based on the establishment of calculating model of reducing gas, reduction mechanism was studied by smelting reduction experiments.

Recovering iron from copper slag by reduction method should inject different kinds of reductants, which arouse much extra energy consumption and contributed to greenhouse gases. The conversion of biomass by biomass pyrolysis is a good approach to utilization of agricultural wastes, and it increases the potential usefulness of biomass as a renewable resource [19–21]. Biomass pyrolysis produces fuel gases and fixed carbon. As one of the production during pyrolysis process, fixed carbon could be a potential reductant for the recovery of iron from copper slag. With the variations in chemical compositions of different biomass samples as reductants, the reduction reaction steps and kinetics of reaction are different.

On the other hand, reduction process of iron oxides leads to mass loss because the reducible oxygen in the crystalline structure of iron oxides will escape as CO or CO$_2$. Thus, the reduction degree of iron ore oxides can be reflected by the degree of mass loss. Studies about reduction kinetics of iron ore oxides have been conducted by thermogravimetric analysis method [22–27]. Lin [24] studied the kinetics of direct reduction of artificial chrome iron ore by isothermal and non-isothermal methods using TG and determined the mechanism functions for different periods. And the reduction of hematite was in the sequence of Fe$_2$O$_3$, Fe$_3$O$_4$, FeO (FeAl$_2$O$_4$, Fe$_2$SiO$_4$) and Fe. Dang [25] used hydrogen as reductant and studied the kinetics and mechanism of ilmenite powders. Sun [26] studied coal-based reduction mechanism functions of oolitic iron ore by TG, X-ray diffraction (XRD) and scanning electron microscope (SEM). Akhtar [27] used lignite char as the reductant and studied the direct reduction process of hematite, completed in iron oxide pellets. Lignite char could successfully reduce hematite to iron at 1073–1273 K.

In this paper, the present study was to investigate the reduction kinetics and reduction ratio of copper slag with three typical biomasses as reducing agent by TG. The reduction process of the mixture of copper slag and biomass was discussed during the heating process. Effects of the biomass type, biomass addition, heating rate and CaO addition on iron reduction ratio from copper smelting slag were studied. The mechanism functions and reaction kinetics were calculated.

Experimental and methods

Materials

Before experiment, the copper slag samples were crushed to the size smaller than 150 μm. The CaO sample was calcined from CaCO$_3$ (AR) at 1273 K for 10 h. The biomass materials are corncob, pine sawdust, and straw from Liaoning province of China (abbreviated as CN, PE, and SW, respectively). The samples were dried in vacuum drying oven at 353 K for 12 h, then ground by crusher, finally sieved to 250 μm for experiments.

The compositions of copper slag used in experiments are shown in Table 1. From Table 1, FeO, SiO$_2$ and Fe$_3$O$_4$ are the main compositions for copper slag. The element content of Fe (MFe, Fe^{2+} and Fe^{3+}) reaches to 44.08 % in copper slag. The phases in raw materials were identified by X-ray diffractometer (Shimadzu, XRD-7000) using Cu-K_α radiation operated at 30 kV and 40 mA, and diffraction data was recorded continuous scanning with a step of 2°

min^{-1}. Figure 1 represents XRD patterns of the waste slag before the reduction reaction. From Fig. 1, iron in copper slag is in the phase of fayalite (Fe_2SiO_4) and magnetic (Fe_3O_4). The impurity peaks of XRD patterns are the other low content compositions. The analytical data (proximate analysis, components analysis and ultimate analysis) for the biomass samples are shown in Table 2. From the proximate analysis, PE has the highest content of volatile and CN has the highest content of fixed carbon. From the components analysis, it can be seen that hemi-cellulose, cellulose, and lignin are the three main components of the biomass. And the contents of cellulose, lignin for PE is highest. By ultimate analysis, the content of carbon in PE is higher than CN and PE.

Apparatus and methods

A NETZSCH STA409PC thermogravimetric analyzer was employed. The biomass, copper slag and CaO were mixed thoroughly and placed in the high purity aluminum crucible. The protective gas was Ar and, its flow rate was 30 mL min^{-1}, controlled by flow meters. In each experiment, considering the restriction of apparatus on temperature, about 10 mg samples were heated from 298 to 1723 K at a heating rate of 10, 20, or 40 K min^{-1} and kept the reaction temperature of samples at 1723 K for 30 min, respectively. During the heating process, the pyrolysis reaction of biomass occurred firstly and the reduction reactions of copper slag with fixed carbon took place after. The experimental conditions are shown in Table 3. Biomass/Slag and CaO/Slag are abbreviated as B/S and CaO/S, respectively.

During reduction process, copper slag is reduced by fixed carbon, produced from biomass pyrolysis. CO and
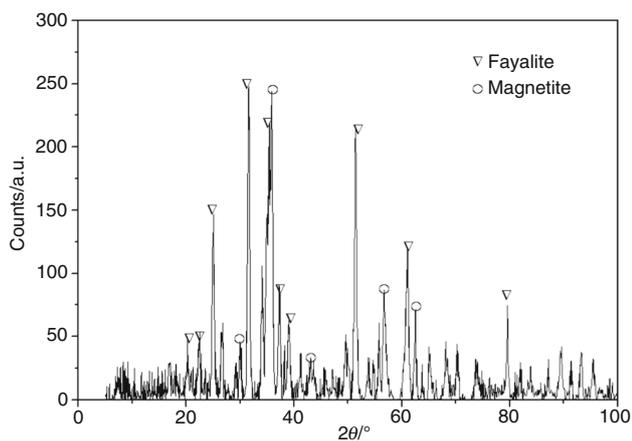

Fig. 1 The picture of X-ray diffraction spectrogram of copper slag

Table 2 Properties of three biomass materials

Samples	CN	PE	SW
Proximate analysis/mass%			
Moisture	6.07	3.81	6.84
Volatiles matter	73.54	79.01	67.90
Ash	3.43	2.17	9.36
Fixed carbon	16.96	15.01	15.90
Components analysis/mass%			
NDF	17.93	10.99	32.02
Hemicellulose	18.74	5.90	18.38
Cellulose	53.69	58.88	39.68
Lignin	8.75	23.42	7.38
Ultimate analysis/mass%			
Nitrogen	1.65	0.15	0.61
Carbon	41.34	48.28	45.16
Hydrogen	5.769	6.17	5.928
Sulfur	0.125	0.082	0.069

Table 3 Experimental conditions

Biomass	B/S	CaO/S	Heating rate/K min^{-1}
CN	0.5:1	0:1	10
PE	1:1	0.15:1	20
SW	2:1	0.3:1	40
		0.45:1	

CO_2 are generated in the reduction reaction of copper slag by solid carbon and CO gas. The reduction of solid carbon played the main role in the reduction, and the rate of reduction by CO gas was only 5–10 % of that by solid carbon in molten slag, which was verified by Bafghi, Sugata and Li [28–30]. Reduction of iron oxides leads to mass loss because the reducible oxygen in the crystalline structure of iron oxides will escape as CO. Thus, the degree of mass loss reflects the reduction degree of iron ore oxides. In the present investigation, Wang [31] modified Eq. (1) and determined the degree of reduction in iron ore-coal composite pellets. Sah [32] and Sun [26] modified Eq. (1) and calculated the coal-based reduction degree of iron ore by this method. Therefore, mass loss method could be used to determine the degree of reduction. The recovery of iron from copper slag could be determined by mass loss of sample during the reduction process.

$$r = \frac{16}{28} \times \left(\frac{f_{w1} - (f_{coal} \times f_{vm} \times f_{vr})}{f_{ore} \times \rho_{ore} \times f_o} \right) \times 100\% \qquad (1)$$

where r is the degree of reduction, %; f_{w1} is fractional mass loss; f_{coal} is fraction of coal present in composite pellet; f_{vm} is fraction of volatile matters present in coal; f_{vr} is fraction of volatiles released during reduction at particular temperature; f_{ore} is fraction of ore present in composite pellet; and ρ_{ore} is the purity of iron oxide (Fe_2O_3).

In order to obtain the actual mass loss of reducible oxygen in copper slag, three samples were measured at the same experimental conditions in each reduction experiment. The relationships in mass and description of sample A, B and C are shown in Fig. 2 and Table 4. Sample A is the mixture of copper slag, CaO and biomass, which were mixed sufficiently. And the mass loss of sample A during reduction is caused by loss of fixed carbon, loss of reducible oxygen in Fe_3O_4 and FeO, loss of volatiles by biomass pyrolysis and loss of trace of volatile in copper slag. Sample B is the mixture of SiO_2 and biomass. The mass of SiO_2 in sample B is equal to the mass of CaO and copper slag in sample A and the mass of biomass in sample B is equal to sample A. And the mass loss of sample B on the same conditions is caused by loss of volatiles by biomass pyrolysis. Sample C is copper slag, and the mass of copper slag in sample A and C is equal. The mass loss of sample C is caused by loss of trace of volatile in copper slag. SiO_2 powder in sample B could eliminate diffusion effects of copper slag on the reduction. The mass of CaO and SiO_2 remain invariant, which was verified in experiments.

Modified by Eq. (1), the reduction degree of copper slag is calculated as follows:

$$r^t = \frac{\frac{16}{28} \times (\Delta_A^t - \Delta_B^t - \Delta_C^t)]}{m_C\left(FeO\% \times \frac{16}{72} + Fe_3O_4\% \times \frac{64}{232}\right)} \times 100\% \qquad (2)$$

where r^t is reduction ratio of copper slag at time of t, %; Δ_A^t, Δ_B^t, Δ_C^t are mass loss of sample A, B and C at reduction time of t, g; m_c is the mass of copper slag before reduction, g; FeO % and Fe_3O_4 % are the chemical contents of FeO and Fe_3O_4 in copper slag, respectively, %.

Results and discussion

Analysis of pyrolysis process and reduction process

In experiments, copper slag, biomass and CaO were mixed in a certain ratio. On account of the complicated components of biomass and copper slag, the chemical reactions are different at different temperature regions. In order to find out the reaction processes of pyrolysis and reduction temperature regions, respectively, thermodynamic calculations combined thermogravimetric curves are carried forward. The productions of biomass pyrolysis mainly include fixed carbon, condensable gas, volatile gas and ash. Among these productions, volatile gas and condensable gas are blown out by Ar, accompanying with decomposition reactions. In consequence, the potential contributed reductants to the reductions of copper slag are fixed carbon, CO and H_2. In copper slag, Fe element occupies the main mass and it is in the shapes of Fe, FeO and Fe_3O_4. Therefore, the reduction reactions of copper slag are the reductions of FeO and Fe_3O_4.

Equations (3)–(8) are the main basic reduction reactions involved in slag system. Multi-step reduction reactions can be superposed by these basic reduction reactions.
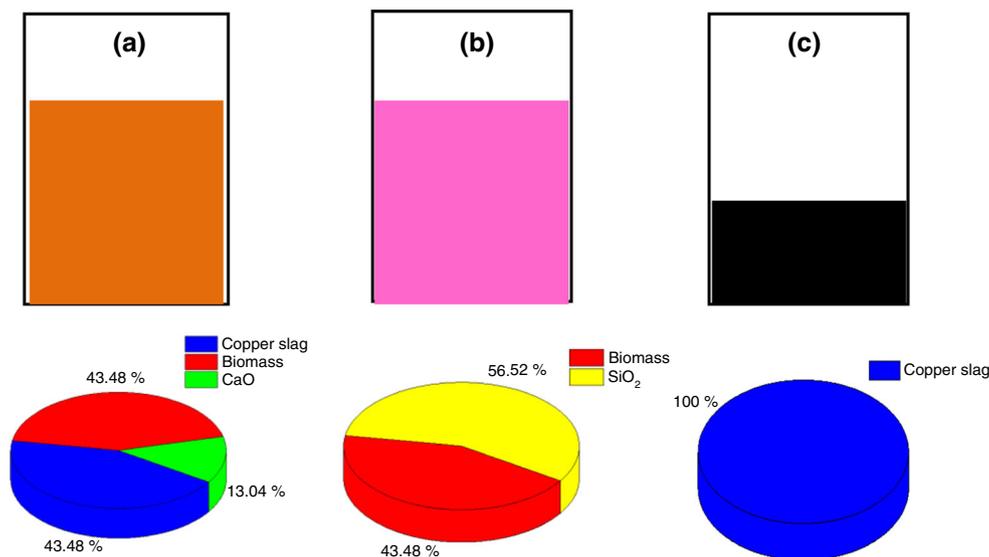

Fig. 2 Samples of TG experiments (B/S = 1:1, CaO/S = 0.3:1). **a** Mixture of copper slag, biomass and CaO; **b** mixture of SiO_2 and biomass; **c** copper slag

Table 4 The relationships of samples A, B and C in mass (B/S = 1:1; CaO/S = 0.3:1)

Samples	Total mass/mg	Copper slag/mg	Biomass/mg	CaO/mg	SiO_2/mg
A	10	4.35	4.35	1.3	0
B	10	0	4.35	0	5.65
C	4.35	4.35	0	0	0

Equations (9) and (10) are gasification reactions between C and CO_2 or H_2O that would take place in reduction reaction system. And the gasification reactions take place above 947 and 973 K, respectively. The all possible gaseous products of these reactions are CO, CO_2 and H_2O, respectively. For instance, the reduction of Fe_3O_4 by fixed carbon is made up with Eqs. (3, 4, 6). By calculating the Gibbs free energy of these reactions, we could make out the degrees of each reaction at different temperature. As shown in Fig. 3, changes of Gibbs free energy for the reduction by C (Eqs. 3, 6) are less than zero and far lower than that by CO and H_2 (Eqs. 4, 5, 7, 8), which means the driving force by C is stronger. What is more, the reaction time of CO and H_2 with copper slag was much shorter than that of fixed carbon during the heating process. And it was also proved by Sugata [29] that when CO gas was blown into molten slag at a 15 times larger than the generation reaction rate of CO, the reduction rate of iron oxide by CO gas was only about 5–10 % of that by solid carbon. Therefore, gasification reactions (Eqs. 9, 10) could be neglected and the main reduction reactions in the experiment are the reduction of copper slag with fixed carbon (Eqs. 3, 6). The initial reaction temperatures of reductions for FeO and Fe_3O_4 are 992 and 959 K (Eqs. 3, 6), respectively. From thermogravimetric curves, the pyrolysis process of biomass and reduction process of copper slag and fixed carbon are represented in Fig. 4. When the temperature was under
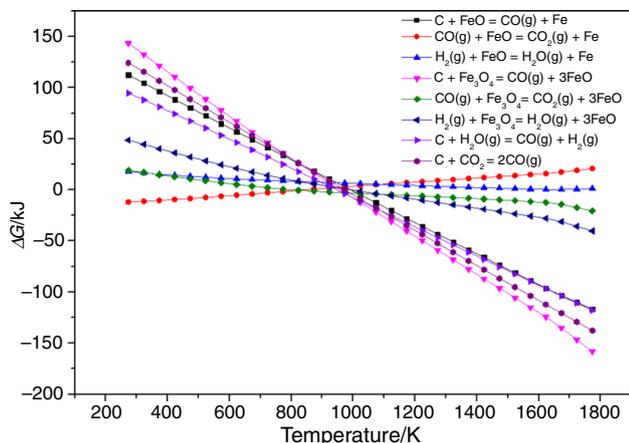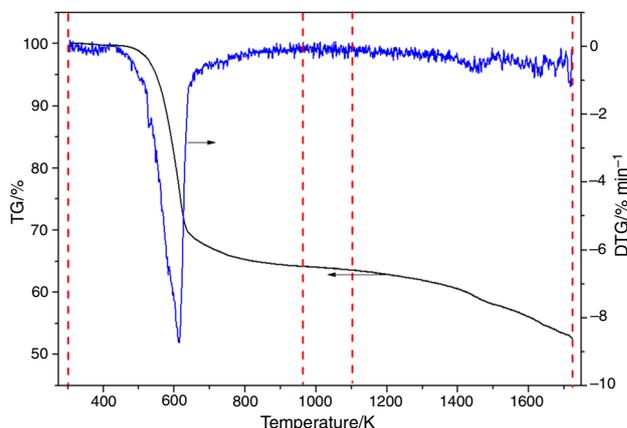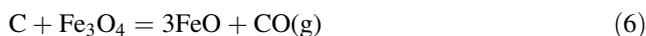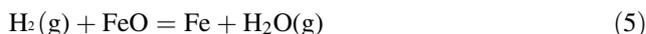

Fig. 4 Thermogravimetric curves of sample (sample A, PE, B/S = 1:1, CaO/S = 0:1)

959 K, mass loss is caused by pyrolysis of biomass. And when the temperature was above 1100 K, mass loss is caused by reduction of copper slag by fixed carbon. The pyrolysis process of biomass has been completed before reduction process. In other words, there is no overlap between the reduction and pyrolysis process.

$$C + FeO = Fe + CO(g) \qquad (3)$$

$$CO(g) + FeO = Fe + CO_2(g) \qquad (4)$$

$$H_2(g) + FeO = Fe + H_2O(g) \qquad (5)$$

$$C + Fe_3O_4 = 3FeO + CO(g) \qquad (6)$$

$$CO(g) + Fe_3O_4 = 3FeO + CO_2(g) \qquad (7)$$

$$H_2(g) + Fe_3O_4 = 3FeO + H_2O(g) \qquad (8)$$

$$C + H_2O(g) = CO(g) + H_2(g) \qquad (9)$$

$$C + CO_2(g) = 2CO(g) \qquad (10)$$

Based on the thermo calculating and thermogravimetric curves analysis above, the whole process of can be divided into three stages:

(a) Drying and pyrolysis of biomass (<959 K). Drying and pyrolysis of biomass with complicated reactions take place in this stage. Hemicellulose, cellulose and lignin depolymerize to monomer firstly, and different kinds of radicals rearranged later, fixed carbon,

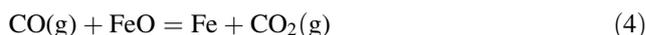**Fig. 3** The Gibbs free energy curves of reduction and gasification reactions in copper slag

ash and pyrolysis gas are generated at last. There is an evident decrease on TG (mass loss) curve from 500 to 700 K and DTG (the rate of mass loss) curve reached a peak at about 620 K.

(b) Pre-reduction. From 959 to 1100 K, the recovery rate of Fe in slag is extremely slow and traces of Fe_3O_4 are involved in the reaction (Eq. 6) and the mass of sample declines slightly.

(c) Reduction reaction. When the temperature is higher than 1100 K, the rate of reduction increases and reaches to stabilization gradually. In this stage, C bond is broken and produces radicals for deoxidation. Reduction of iron oxides in copper slag leads to mass loss because the reducible oxygen in the crystalline structure of iron oxides will escape as CO. The reduction of copper slag is in the sequence of Fe_3O_4, FeO (Fe_2SiO_4) and Fe.

Results of thermogravimetric analysis

Influence of the biomass types on the reduction ratio of molten copper slag

Based on the proximate and components analysis, the composition and fiber structure of three kinds of biomass in this experiment are different. According to Fig. 5, with the increase in the addition of biomass, the reduction ratio of copper slag increases obviously. The results shows that the order of reduction ratios from high to low in biomass type is PE > CN > SW. Compared with CN and SW, PE presents the highest reduction ratio and the reduction ratios of PE, CN and SW reaches to 80.6, 76.1, 60.0 %, respectively, when the mass ratio of biomass/slag is 1:2. Based on component analysis, the content of lignin in PE is highest,
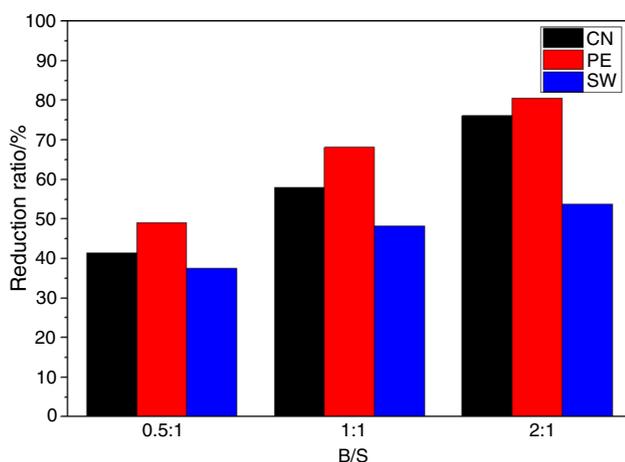
compared with that in CN and SW. Gas yield from lignin is lower than hemicellulose and cellulose, and the lignin is the main component to produce carbon element during the pyrolysis process [33]. For the reduction reaction of copper slag, the ratio of C/O of PE is higher than that of CN and SW under the same conditions.

Influence of heating rate on the reduction ratio of molten copper slag

The heating rate can change the activation energy of reduction reaction and reduction reaction time of copper slag. The rise of heating rate can decrease the activation energy of reduction reaction and promote the reduction rate. Besides, the faster the heating rate is, the shorter the reaction time would be. The heating rates of samples were 10, 20 and 40 K min^{-1} in the experiment. As shown in Fig. 6, with the increase in heating rate, the reduction ratio of copper slag decreases. The extent of variation of reduction ratio of PE and SW are greater than CN. And when the heating rates changed from 10 to 40 K min^{-1}, the reduction ratio of copper slag for CN changes less than PE and SW. Possibility, the fiber of CN is smaller than PE and SW, and larger reaction surface area leads to faster reaction. Therefore, the reduction reaction time for PE and SW should be more than 50 min at least, which was longer than CN.

Influence of the CaO addition on the reduction ratio

Additives (CaO, MgO, SiO_2, Al_2O_3, MnO, NiO, Cr_2O_3) have influence on the reduction of Fe_2O_3, which was investigated in details by Geassy, Nasr, Khedr, Hessein et al. [34–37]. CaO has remarkable promotion influence on the reduction of iron oxides for its better combining capacity with SiO_2 in slag [5]. And as slag
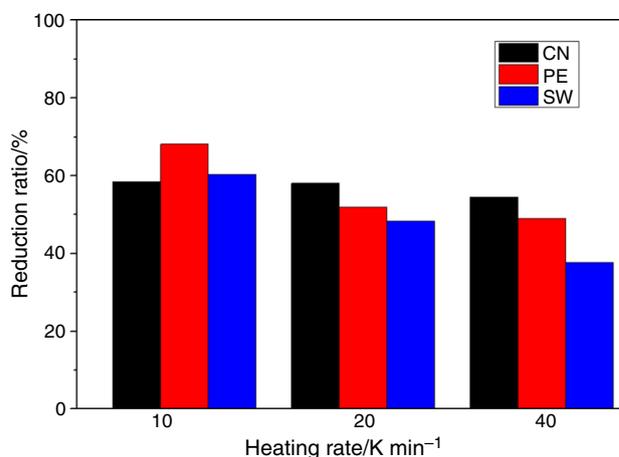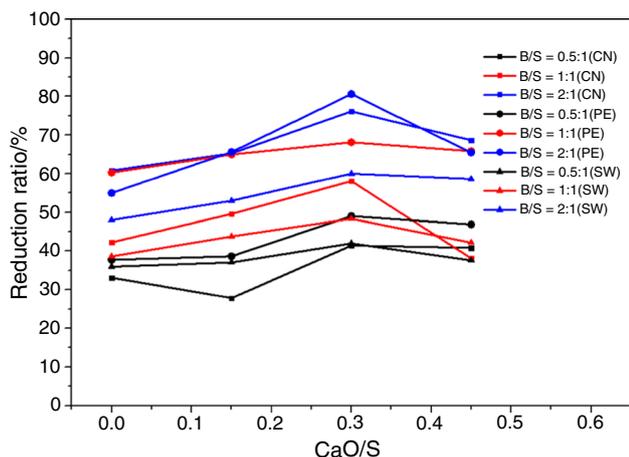

Fig. 5 Effects of the addition and the types of biomasses on reduction ratio

Fig. 6 The effects of heating rate on the reduction ratio

Fig. 7 The effects of CaO addition on the reduction ratio of copper slag

Fig. 9 Curves of linear regression of different models (PE, >100 mesh number, 20 K min^{-1})
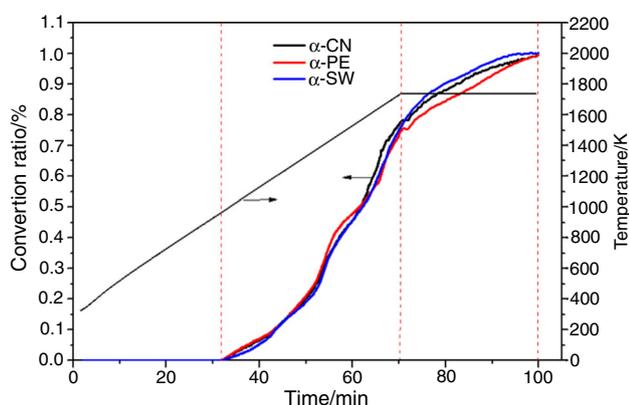

Fig. 8 Conversion ratio curves of three kinds of biomasses (B/S = 1:1, CaO/S = 0.3:1)

former, CaO is applied widely in smelting industry. CaO is doped in sample, and the promotion of CaO in chemical reaction rate for copper slag is studied in this article. Figure 7 reflects the effects of CaO addition on the reduction ratio of copper slag. The total development trends of PE CN and SW are identical. When the mass ratios of CaO/S are 0.15:1, 0.3:1 and 0.45:1, the reduction ratios of copper slag are enhanced in varying degrees. With the increase in CaO addition, the reduction ratio of copper slag increases and then declines and it reaches a peak at 0.3:1. Based on the coexistence theory of slag structure, CaO participates in Reactions (11–13) and promotes Reaction (14) to move backward, which promotes the separation of Fe and SiO$_2$ sequentially. The separation of them is a favorable condition for the reduction of copper slag. However, when the addition of CaO is excessive, CaO exists as insoluble phase and it adds the viscosity of molten slag. Consequently,
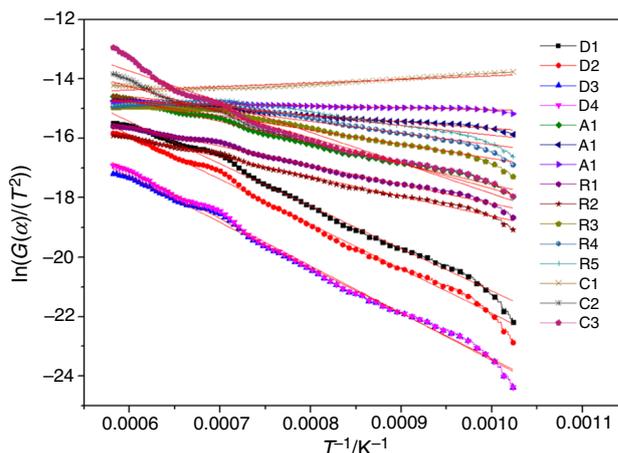
excessive CaO worsens the dynamic condition of reactions in molten slag.

$$Ca^{2+} + O^{2-} + SiO_2 = CaO \cdot SiO_2 \tag{11}$$

$$2(Ca^{2+} + O^{2-}) + SiO_2 = 2CaO \cdot SiO_2 \tag{12}$$

$$3(Ca^{2+} + O^{2-}) + SiO_2 = 3CaO \cdot SiO_2 \tag{13}$$

$$2(Fe^{2+} + O^{2-}) + SiO_2 = 2FeO \cdot SiO_2 \tag{14}$$

Kinetics analysis

Non-isothermal and isothermal kinetics study methods were carried out on the rate and mechanism of gaseous and solid reduction of iron oxides. Avrami–Erofeev Equation model, nucleation and growth model, phase boundary chemical reaction model and diffusion model were determined in different periods for the reduction of iron ore oxides [14–17]. In this paper, based on Coats–Redfern method [38], the kinetics of reduction could be described as follows:

$$\frac{d\alpha}{dt} = kf(\alpha) \tag{15}$$

The conversion ratio α, reaction rate k and heating rate β are expressed as follows:

$$\alpha = \frac{m_0 - m_t}{m_0 - m_1} \tag{16}$$

$$k = A \exp\left(-\frac{E}{RT}\right) \tag{17}$$

$$\beta = \frac{dT}{dt} \tag{18}$$

Equation (15) can be converted to:

Table 5 Reaction kinetics models

Models	Symbol	Rate equation $f(\alpha)$	Reaction mechanism equation $G(\alpha)$
One-dimension diffusion	D_1	$1/2\alpha$	α^2
Two-dimension diffusion (cylindrical symmetry)	D_2	$[-\ln(1-\alpha)]^{-1}$	$\alpha + (1-\alpha)\ln(1-\alpha)$
Three-dimension diffusion (cylindrical symmetry)	D_3	$(3/2)[(1-\alpha)^{-1/3}-1]^{-1}$	$1 - (2/3)\alpha] - (1-\alpha)^{2/3}$
Three-dimension diffusion (spherical symmetry)	D_4	$(3/2)(1-\alpha)^{2/3}[1-(1-\alpha)^{2/3}]^{-1}$	$[1-(1-\alpha)^{1/3}]^2$
Random nucleation ($n = 1$)	A_1	$1-\alpha$	$-\ln(1-\alpha)$
Random nucleation ($n = 2$)	A_2	$2(1-\alpha)[-\ln(1-\alpha)]^{1/2}$	$[-\ln(1-\alpha)]^{1/2}$
Random nucleation ($n = 3$)	A_3	$3(1-\alpha)[-\ln(1-\alpha)]^{2/3}$	$[-\ln(1-\alpha)]^{1/3}$
Shrinking core (cylindrical symmetry)	R_1	$2(1-\alpha)^{1/2}$	$1-(1-\alpha)^{1/2}$
Shrinking core (spherical symmetry)	R_2	$3(1-\alpha)^{2/3}$	$1-(1-\alpha)^{1/3}$
Shrinking core ($n = 2$)	R_3	$1/2(1-\alpha)^{-1}$	$1-(1-\alpha)^2$
Shrinking core ($n = 3$)	R_4	$1/3(1-\alpha)^{-2}$	$1-(1-\alpha)^3$
Shrinking core ($n = 4$)	R_5	$1/4(1-\alpha)^{-3}$	$1-(1-\alpha)^4$
Chemical reaction ($n = 3/2$)	C_1	$2(1-\alpha)^{3/2}$	$(1-\alpha)^{-1/2}$
Chemical reaction ($n = 2$)	C_2	$(1-\alpha)^2$	$(1-\alpha)^{-1}-1$
Chemical reaction ($n = 3$)	C_3	$(1-\alpha)^3$	$1/2[(1-\alpha)^{-2}-1]$
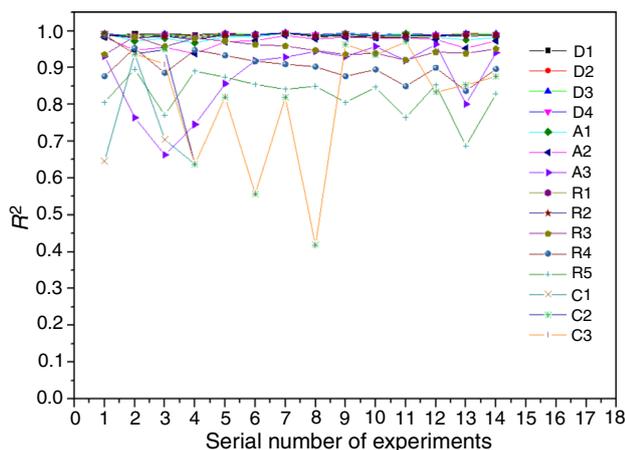
Fig. 10 Curves of R-square of different models (PE)

$$\frac{d\alpha}{f(\alpha)} = \frac{A}{\beta}\exp\left(-\frac{E}{RT}\right)dT \qquad (19)$$

where α is the conversion ratio, %; m_0 m_1 and m are the sample mass at the start, the end and at time t respectively, g; k is the chemical reaction rate constant; β is the heating rate, K min^{-1}; $f(\alpha)$ is the mechanism function; A is the pre-exponential factor, min^{-1}; E is the activation energy, kJ mol^{-1}; and R is the universal gas constant, kJ mol^{-1} K^{-1}.

As we can see from Fig. 8, the trends of conversion ratio curves for three kinds of biomasses are consistent. Considering the restriction of apparatus on temperature, the samples were heated from 298 to 1723 K at a heating rate (20 K min^{-1} in Fig. 8) and kept the reaction temperature

of samples at 1723 K for 30 min, respectively. Reduction reaction happened in heating period and constant temperature period. The dynamic kinetics is calculated in heating period (1100–1723 K).

Then by integrating Eq. (17), we can get:

$$G(\alpha) = \int_0^\alpha \frac{d\alpha}{f(\alpha)} = \int_0^T \frac{A}{\beta}\exp\left(-\frac{E}{RT}\right)dT \qquad (20)$$

For convenient, the term of $u = E/RT$ is introduced:

$$\int_0^T \frac{A}{\beta}\exp\left(-\frac{E}{RT}\right)dT = -\frac{E}{R}\int_u^\infty e^{-u}u^{-2}du$$

$$\approx \frac{E}{R}\left(1-\frac{2}{u}\right)u^2 e^{-u} \quad [38] \qquad (21)$$

$$\ln\left[\frac{G(\alpha)}{T^2}\right] \approx \ln\left[\frac{AR}{\beta E}\left(1-\frac{2RT}{E}\right)\right] - \frac{E}{RT} \qquad (22)$$

As the term of $2RT/E$ is far less than 1 and can be neglected, Eq. (22) can be simplified as:

$$\ln\left[\frac{G(\alpha)}{T^2}\right] \approx \ln\left(\frac{AR}{\beta E}\right) - \frac{E}{RT} \qquad (23)$$

As calculated above, the relationship between T and $G(\alpha)/T^2$ in Eq. (23) is transformed into a linear function. According to Fig. 9, by linear fitting of 15 mechanism functions in Table 5 [39], the linear correlation coefficient R^2 and regression square sum RSS are obtained. Compared with other models, the relevance of D1, D2, D3, D4, A1, R1 and R2 are above 0.98 as shown in Fig. 10. The serial numbers of experiments in Fig. 10 are named by the

Table 6 The RSS of the different mechanism models for reduction of copper slag

B/S	0.5:1				1:1			
(a)								
CaO/S	0:1	0.15:1	0.3:1	0.45:1	0:1	0.15:1	0.3:1	0.45:1
Heating rate/K min^{-1}	20	20	20	20	20	20	20	20
D1	169.94	77.48	70.44	108.08	75.44	120.64	84.54	261.86
D2	201.51	123.27	84.39	160.76	87.13	128.17	65.82	231.70
D3	217.88	147.87	96.00	189.16	96.98	136.59	62.10	224.47
D4	258.02	209.33	130.52	260.53	126.08	166.37	62.25	224.54
A1	77.23	72.78	46.52	89.71	42.96	53.45	17.89	60.27
R1	52.58	33.25	22.89	43.06	23.47	31.76	16.03	54.80
R2	59.09	43.51	28.19	55.09	27.87	36.16	15.14	53.72
B/S	2:1				1:1			
(b)								
CaO/S	0:1	0.15:1	0.3:1	0.45:1	0.3:1	0.3:1	0.3:1	
Heating rate/K min^{-1}	20	20	20	20	10	20	40	
D1	230.96	382.30	239.04	330.23	124.64	84.54	171.16	
D2	170.52	318.50	178.72	281.15	117.83	65.82	135.74	
D3	151.34	297.03	157.18	267.81	124.30	62.10	124.02	
D4	123.59	274.70	122.51	287.18	162.40	62.25	105.81	
A1	28.51	70.09	24.97	112.36	65.89	17.89	25.08	
R1	41.19	73.34	42.38	64.21	29.94	16.03	34.78	
R2	35.03	68.13	35.19	67.38	35.92	15.14	30.66	
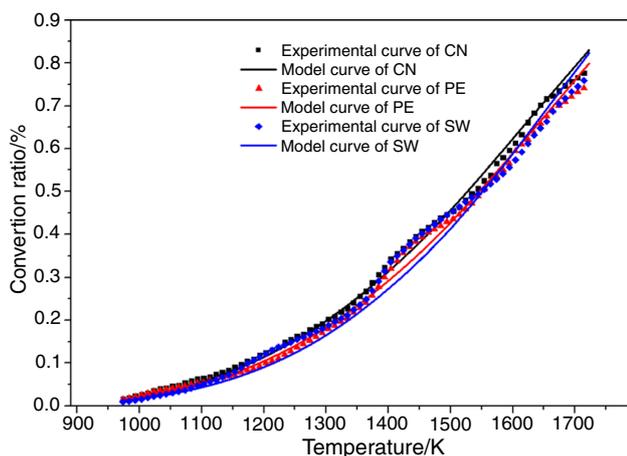
Fig. 11 Comparison between the model and experimental curves of CN, PE and SW under 20 K min^{-1}

sequence of experiments in Table 6a. And as shown in Table 6, the RSS calculated results of R1 model are lower than others.

Based on the calculations of fifteen chemical mechanism functions above, the reduction reaction of copper slag by biomass is confirmed well with shrinking core model (R1). Therefore, the kinetic equation is established as:

$$\frac{\mathrm{d}\alpha}{\mathrm{d}T} = \frac{A_i}{\beta}\left(-\frac{E_i}{RT}\right)[2(1-\alpha)^{1/2}] \qquad (24)$$

where E_i and A_i are activation energy and pre-exponential factor in different conditions, respectively. The results of dynamics model parameters are shown in Table 7. On the one hand, as discussed above, the addition of CaO could promote Reaction (14) to move backward, which accelerates the separation of Fe and SiO_2 sequentially; on the other hand, the addition of biomass and CaO increases slag viscosity and changed dynamical condition to some extent. Due to the effects of the separation of Fe and SiO_2 and changes of viscosity, the effects of CaO on the kinetic parameters are not in order clearly. With the increase in addition of biomass, the activation energy of reactions increases gradually. And similar to the pyrolysis of biomass, with the increase in heating rate, the activation energy of reduction reaction by three kinds of biomass decreased gradually.

In order to verify the accuracy of calculation results, comparison of conversion ratio between the model and experimental curves is discussed as shown in Fig. 11. As a whole, the conversion ratio calculated by R1 model achieves high conformity with thermogravimetric experiments results. With the increase in temperature, the

Table 7 The results of reduction dynamics model parameters of copper slag

B/S	CaO/S	Heating rate/K min^{-1}	E/kJ mol^{-1}	A/min^{-1}
(a) CN				
0.5:1	0:1	20	53.41	1.1773
	0.15:1	20	50.31	0.9544
	0.3:1	20	53.93	1.9226
	0.45:1	20	48.45	0.9447
1:1	0:1	20	64.48	3.7559
	0.15:1	20	57.65	2.3443
	0.3:1	20	51.92	1.5461
	0.45:1	20	50.27	0.9957
2:1	0:1	20	59.79	2.8913
	0.15:1	20	60.15	3.3061
	0.3:1	20	64.14	5.7917
	0.45:1	20	61.80	4.9882
1:1	0.3:1	10	68.81	3.6006
		20	51.92	1.5461
		40	44.03	1.0959
(b) PE				
0.5:1	0:1	20	45.03	0.5237
	0.15:1	20	49.10	0.8792
	0.3:1	20	45.00	0.6608
	0.45:1	20	49.70	0.9750
1:1	0:1	20	52.02	1.1104
	0.15:1	20	56.03	2.0624
	0.3:1	20	53.49	1.4565
	0.45:1	20	65.98	5.6257
2:1	0:1	20	62.54	3.8937
	0.15:1	20	74.38	13.6928
	0.3:1	20	60.10	1.9609
	0.45:1	20	84.59	54.6791
1:1	0.3:1	10	64.00	2.5970
		20	53.49	1.4565
		40	47.99	1.3229
(c) SW				
0.5:1	0:1	20	47.76	0.8190
	0.15:1	20	53.01	1.1280
	0.3:1	20	52.76	1.0449
	0.45:1	20	50.33	0.9167
1:1	0:1	20	56.68	1.5994
	0.15:1	20	62.18	2.9017
	0.3:1	20	60.24	2.6620
	0.45:1	20	55.23	1.9415
2:1	0:1	20	61.99	3.1208
	0.15:1	20	65.76	5.6687
	0.3:1	20	70.53	9.7846
	0.45:1	20	69.92	9.9316
1:1	0.3:1	10	73.20	9.8340
		20	60.24	2.6620
		40	53.18	2.1586

conversion rate of reduction increases gradually. When the temperature is between 1400 and 1500 K, phase transition of copper slag causes the short increase in conversion rate and return to normal level after.

Conclusions

The results obtained in this work indicate that biomass would be a potential good reductant for the reduction of copper slag. During heating process, the reduction reaction of copper slag and biomass can be divided into three stages, drying and pyrolysis of biomass process (<959 K), pre-reduction process (959–1100 K) and reduction reaction process (>1100 K).

Compared with CN and SW, PE had the largest reduction ratios and the reduction ratios of PE, CN and SW reached to 80.6, 76.1, and 60.0 %, respectively, when the mass ratio of B/S was 2:1. CaO had promotion effects on the reduction reaction. With the increase in CaO, the reduction ratio of copper slag increased firstly and reached a peak when CaO/S was 0.3:1, and then it declined due to the increase in viscosity. The reduction reaction of copper slag by biomass confirmed well with shrinking core model (R1). The activation energy of reactions increased gradually with the increase in biomass. With the increase in heating rate, the activation energy of reduction reaction decreased gradually. On account of the separation of Fe and SiO$_2$ and changes of viscosity of molten copper slag affected by CaO, the effects of CaO on the activation energy are not in order clearly.

References

1. Copper: preliminary date for September 2015. ICSG. http://www.icsg.org.
2. Shi C, Meyer C, Behnood A. Utilization of copper slag in cement and concrete. Resour Conserv Recycl. 2008;52(10):1115–20.
3. de Rojas MIS, Rivera J, Frias M, Marin F. Use of recycled copper slag for blended cements. J Chem Technol Biotechnol. 2008;83(3):209–17.
4. Liu H, Lu H, Chen D, Wang H, Xu H, Zhang R. Preparation and properties of glass–ceramics derived from blast-furnace slag by a ceramic-sintering process. Ceram Int. 2009;35(8):3181–4.
5. Heo JH, Kim B-S, Park JH. Effect of CaO addition on iron recovery from copper smelting slags by solid carbon. Metall Mater Trans B. 2013;44(6):1352–63.

6. Zhang HW, Shi SX, Zhang B, Hong X. Reduction of molten copper slags with mixed CO-CH$_4$-Ar gas. Metall Mater Trans B. 2013;45(2):582–9.

7. Siwiec G, Oleksiak B, Matula T, Socha L, Stanek W. Reduction of copper slag with the use of carbon granulates. Metallurgy. 2014;53(4):585–7.

8. Zhang J, Qi YH, Yan DL, Xu HC. A new technology for copper slag reduction to get molten iron and copper matte. J Iron Steel Res Int. 2014;22(5):396–401.

9. Hu JH, Wang H, Li L. Recovery of iron from copper slag by smelting reduction. 2011 International conference on computer, electrical and systems sciences, and engineering, Information Engineering Research Institute, China: 2011; 541–4.

10. Zhang LN, Zhang L, Wang MY, Sui ZT. Research on the oxidization mechanism in CaO–FeOx–SiO$_2$ slag with high iron content. Trans. Nonferrous Met. Soc. China. 2005; 15(4): 1-6.

11. Gyurov S, Rabadjieva D, Kovacheva D, Kostova Y. Kinetics of copper slag oxidation under nonisothermal conditions. J Therm Anal Calorim. 2014;116(2):945–54.

12. Bruckard WJ, Somerville M, Hao F. The recovery of copper, by flotation, from calcium-ferrite-based slags made in continuous pilot plant smelting trials. Miner Eng. 2004;17(4):495–504.

13. Warczok A, Riveros G. Slag cleaning in crossed electric and magnetic fields. Miner Eng. 2007;20(1):34–43.

14. Seo K, Fruehan R. Reduction of FeO in slag with coal char. Transactions of the Iron & Steel Institute of Japan. 2000;40(1):7–15.

15. Min DJ, Han JW, Chung WS. A study of the reduction rate of FeO in slag by solid carbon. Metallurgical and Materials Transitions. 1999;30B:215–21.

16. Sarma B, Cramb AW, Fruehan RJ. Reduction of FeO in smelting slags by solid carbon experimental results. Metallurgical and Materials Transactions. 1993;27(5):717–30.

17. Utigard T, Sanchez G, Manriquez J, Lurashi A, Diaz C, Cordero D, Almendras E. Reduction kinetics of liquid iron oxide-containing slags by carbon monoxide. Metallurgical and Materials Transactions. 1997;28B:821–6.

18. Nagasaka T, Hino M, Ban-Ya S. Interfacial kinetics of hydrogen with liquid slag containing iron oxide. Metallurgical and Materials Transactions. 2000;30B:945–55.

19. McKendry P. Energy production from biomass (part 3): gasification technologies. Bioresource Technol. 2002;83(1):55–63.

20. Bridgwater AV, Meier D, Radlein D. An overview of fast pyrolysis of biomass. Org Geochem. 1999;30(12):1479–93.

21. Han J, Kim H. The reduction and control technology of tar during biomass gasification/pyrolysis: an overview. Renew Sust Energ Rev. 2008;12(2):397–415.

22. Reddy BR, Murthy BVR, Swamy YV, Ray HS. Correlation of Nickel Extraction with Iron Reduction in Oxidic Nickel Ore by a Thermogravimetric Method. Thermochim Acta. 1995;264:185–92.

23. Chakraborty A. Kinetics of the reduction of hematite to magnetite near its Curie transition. J Magn Magn Mater. 1999;204(1–2):57–61.

24. Lin Q, Liu R, Chen N. Kinetics of direct reduction of chrome iron ore. J Therm Anal Calorim. 1999;58(2):317–22.

25. Dang J, Zhang GH, Chou KC. Kinetics and mechanism of hydrogen reduction of ilmenite powders. J Alloy Compd. 2015;619:443–51.

26. Sun YS, Han YX, Gao P, Wei XC, Li GF. Thermogravimetric study of coal-based reduction of oolitic iron ore: kinetics and mechanisms. Int J Miner Process. 2015;143:87–97.

27. Akhtar K, Tahmasebi A, Tian L, Yu J, Lucas J. An experimental study of direct reduction of hematite by lignite char. J Therm Anal Calorim. 2015;123(2):1111–8.

28. Bafghi MS, Fukuda M, Ito Y, Yamada S, Sano M. Effect of CO gas formation on reduction rate of iron oxide in molten slag by graphite. Transactions of the Iron & Steel Institute of Japan. 1993;33(11):1125–30.

29. Sugata M, Sugiyama T, Kondo S. Reduction of iron-oxide contained in molten slags with solid carbon. Transactions of the Iron and Steel Institute of Japan. 1974;14(2):88–95.

30. Li Y, Ratchev IP, Lucas JA, Evans GM, Belton GR. Rate of interfacial reaction between liquid iron oxide and CO-CO$_2$. Metallurgical and Materials Transactions B. 2000;31B:1049–58.

31. Wang Q, Yang Z, Tian J, Li W. Mechanisms of reduction in iron ore-coal composite pellet. Ironmaking Steelmaking. 1997;24(6):457–60.

32. Sah R, Dutta SK. Kinetic Studies of Iron Ore-Coal Composite Pellet Reduction by TG–DTA. Trans Indian Inst Met. 2011;64(6):583–91.

33. Wang Y, Wang HH, Zhu F. Theoretical analysis on thermal pyrolysis of major compositions in tree leaves. Scientia Silvae Sinicae. 2012;48(11):99–107.

34. EL-Geassy AA. Reduction of CaO and/or MgO-doped Fe$_2$O$_3$ compacts with carbon monoxide at 1173-1473 K. ISIJ International. 1996. 36 (11): 1344-53.

35. EL-Geassy AA. Gaseous reduction of MgO-doped Fe$_2$O$_3$ compacts with carbon monoxide at 1173-1473 K. ISIJ International. 1996. 36 (11): 1328-37.

36. Nasr MI, Omar AA, Khedr MH. EI-Geassy AA. Effect of nickel oxide doping on the kinetics and mechanism of iron oxide reduction. ISIJ Int. 1995;35(9):1043–9.

37. Hessein M, Kashawaya Y, Ishi K, et al. Sintering and heating reduction processes of alumina containing iron ore samples. Ironmaking Steelmaking. 2008;35(3):191–204.

38. Coats AW, Redfern JP. Kinetic parameters from thermogravimetric data. Nature. 1964;201(1):68–9.

39. Li C, Suzuki K. Kinetic analyses of biomass tar pyrolysis using the distributed activation energy model by TG/DTA technique. J Therm Anal Calorim. 2009;98(1):261–6.